Organosilane coatings applied on bronze:

influence of UV radiation and thermal cycles on the protectiveness

C.Chiavari[1*], A.Balbo[2] , E.Bernardi[3], C.Martini[4], F.Zanotto[5], I.Vassura[3], M.C.Bignozzi[6], C.Monticelli[2]

[1] C.I.R.I. (Centro Interdipartimentale di Ricerca Industriale)

Meccanica Avanzata e Materiali

Università di Bologna, Via Risorgimento 2, 40136 Bologna (Italy, email:

cristina.chiavari@unibo.it

[2] Centro d

i Studi sulla Corrosione e Metallurgia "A. Daccò", Università di Ferrara, Via Saragat 1,

44122 Ferrara, Italy, email: mtc@unife.it

[3] Dipartimento di Chimica Industriale "Toso Montanari",

Università di Bologna, Via Risorgimento 4, 40136 Bologna (Italy), email:

elena.bernardi@unibo.it

[4]Dipartimento di Ingegneria Industriale,

Università di Bologna, Via Risorgimento 4, 40136 Bologna (Italy), email:

carla.martini@unibo.it

[5] Terra&Acqua Tech, University of Ferrara,

Via Saragat 1, 44122 Ferrara, Italy, email: federica.zanotto@unife.it

[6]Dipartimento di Ingegneria Civile, Chimica, Ambientale e dei Materiali

Università di Bologna, Via Terracini 28, 40131 Bologna (Italy), email:

maria.bignozzi@unibo.it

*corresponding author, phone: +390512093464

Abstract

3-mercapto-propyl-trimethoxy-silane (PropS-SH) coatings, with or without the addition of three types of oxide particles (CeO_2 (nano-sized), TiO_2 (nano-sized) and La_2O_3 (micro-sized)), were applied on quaternary bronze (Cu-Sn-Zn-Pb) and tested through natural and artificial exposures. In particular, uncoated and coated samples were exposed both in the coastal town of Rimini (Italy) under sheltered/unsheltered conditions and in a climatic chamber where the samples underwent temperature/UV cycles, at constant humidity. The sample surfaces were periodically characterized by SEM, EDS, micro-Raman, FTIR and XRD techniques. Moreover, during natural exposures, the leaching rain was monthly collected, in order to evaluate the release of the alloying metals from bronze by Atomic Absorption Spectrometry (AAS). The results showed that micro-scale cracking and spalling phenomena took place during natural exposure, partly limiting the protective efficiency of the organosilane coating. In fact, UV radiation has a strong influence on coating performance, inducing structural modifications of the polymer. Oxide particle- and especially TiO_2-charged coatings proved to be more resistant to UV degradation.

Keywords: organic coatings; bronze; atmospheric corrosion; UV degradation; IR spectroscopy; thermal analysis.

1. Introduction

Bronze alloys have been widely used since ancient times to produce artifacts, sculptures and architectonic elements that are still exposed outdoors to different weather and pollution conditions [1,2]. The conservation of these works of art has been commonly tackled with the use of protective treatments and coatings, which are requested to be efficient in retarding the corrosion attack and maintaining the original appearance. However, natural weathering may impair the long-term persistence of their protectiveness, ease of maintenance as well as visual aspect and unpleasant colour changes (yellowing) can strongly alter the artwork.

Nowadays, protective coatings are often based on acrylic resins, fluoropolymers and waxes, containing or not containing corrosion inhibitors. In particular, Incralac® (a solution of methyl-methacrylate/ethyl-methyl-acrylate copolymer, containing benzotriazole), Soter® (a commercial product consisting of 20-24 wt% crystalline wax, BTA and synthetic organic polymer, dispersed in turpentine and ether), various microcrystalline waxes dispersed in white spirit or double-layer systems, such as Incralac® + wax, have been widely used [3-6]. Fluoropolymers have also been used and tested as single coating systems or as topcoats because of their high resistance to degradation [6,7]

Organosilane coatings attracted a significant research attention in recent years, due to their protective efficiency towards the corrosion of several alloys [8-11]. Many studies investigated the protective efficiency of silane coatings against copper or bronze corrosion in artificial rain or in solutions containing specific pollutants, mainly chlorides. They are focused on 3-mercapto-propyl-trimethoxy-silane (PropS-SH) [12-17], 3-mercapto-propyl-triethoxy-silane [18], octadecyl-trimethoxy-silane [19], glycidoxy-propyl-trimethoxy-silane [20], γ -aminopropyltriethoxysilane (γ -APS) [21], or bis-[triethoxy-silyl-propyl]tetrasulfide [22]).

However, only few papers consider the coating resistance to environmental stresses, like UV radiation, temperature or dry/wet cycles [6,7,12,14,15], or investigate the corrosion resistance of silane coatings on pre-patinated surfaces [12,14,15,23]. In our previous works [12-15], 3-

mercapto-propyl-trimethoxy-silane (PropS-SH) containing or not containing CeO_2 nanoparticles was tested as a protective coating for quaternary bronze (Cu-Sn-Zn-Pb) exposed to the outdoor atmosphere, within the frame of a research project devoted to the protection of outdoor bronze monuments. According to these studies [12,13], after 20 days of continuous immersion in 3.5 % NaCl solution at 30 °C, PropS-SH afforded inhibiting efficiencies of 70% or 100%, if a room temperature (RT) curing time of 10 or 60 days, respectively, was allowed. Good protection efficiencies were also obtained under artificial outdoor exposure conditions, simulated by Wet&Dry tests (reproducing exposure to stagnant rain) or Dropping tests (reproducing runoff conditions) in artificial acid rain. Under both conditions, PropS-SH showed comparable protective efficiencies when applied on pre-patinated and bare bronze, with inhibiting efficiencies against metal release of about 83-86%. The exposure to runoff conditions induced the formation of a Sn-enriched patina on which the silane coating adhesion was slightly weakened [14,15].

The good protective properties of hydrolyzed PropS-SH coatings are connected to the formation of silanol groups (Si-OH) and to their subsequent condensation in a polymeric dense Si-O-Si network. On copper and copper alloys, surface chemisorption of PropS-SH through metal thiolate (Me-S-C) [16] and metal siloxane (Me-O-Si) bonds [24] ensures desirable adhesion to the metal substrate.

Exposure of organic coatings to UV radiation can produce oxidation of double bonds, polymer segment scission and cross-linking, while high temperature and moisture can produce thermal degradation and hydrolysis [25]. As far as silane films are concerned, according to Bao et al. [26] after UV-irradiation at 185 nm for 30 min in air, PropS-SH films applied on silicon substrates undergo Si-C breaks and SiOH groups formation, while irradiated propyl-trimethoxysilane rather undergoes –COOH formation. Irreversible structural changes also affect hydrocarbon chains (possibly also those bonded to Si atoms in silanes), as under UV exposure they are subjected to photo-oxidation, inducing carbonyl and hydroxyl groups

formation [27-29]. Conversely, silane coatings crosslinked by hexamethoxymethylmelamine resulted stable under UV-exposure [30].

It is reported that the stability and the protective properties of silane films deposited on industrial metallic and non-metallic substrates may be modified by nanoparticle addition. Accelerated weathering tests have shown that silane modification with TiO_2 nanoparticles permitted the preparation of transparent UV-protective coatings for polycarbonate substrates [31]. TiO_2 can be an effective UV absorber, capable to confer significant protection against UV-induced degradation of polymeric coatings, because of rapid attenuation of the radiation intensity by absorption and scattering [32].

On the other side, addition of CeO_2, La_2O_3, TiO_2 nanoparticles to silane coatings appreciably improved their protectiveness against corrosion during continuous immersions in 3.5% NaCl, where after a 10 day curing they increased corrosion inhibiting efficiencies from 70 to 96 - 98% [12]. In the case of CeO_2 and La_2O_3, a specific inhibition of the corrosion of substrates arises, thanks to their partial dissolution within the hydrated silane film and release of inhibiting cations [33,34]. Nanoparticles are also reported to help silane reticulation by forming Si-O-M bonds (with M = Ti [35] or Ce [36]). Finally, nanoparticles (including SiO_2 and ZrO_2, $CeAlO_3$, beside CeO_2) can act as filler in silane coatings, so improving the silane barrier effect against water ingress [33,37,38].

Natural exposures are reputed fundamental to quantify the coating performances in field, because artificial tests necessarily tend to simplify the exposure conditions and do not take into account all the possible environmental stresses. Nevertheless, scarce literature information can be found about natural weathering of coatings on bronze, because these effects are detected in the long period [3,39-41]. One test performed on silane coatings [41] highlighted that, after 8 months, only two from five commercial silane coatings were still very protective and did not alter the surface aspect of bronze. That research did not investigate the degradation mechanism of the coatings.

The aim of this study was to carry out a more complete and reliable evaluation of the protective efficiency of PropS-SH coatings by performing both natural and artificial exposure tests, which take into account the influence of UV radiation/temperature cycles under humid conditions. Specifically, the natural weathering tests were conducted in the coastal town of Rimini (Italy), close to an environmental monitoring station, where uncoated and silane-coated bronze samples were exposed in sheltered and unsheltered conditions with respect to sunlight and rain flow. Some PropS-SH coatings also contained oxide particles (CeO_2, La_2O_3, TiO_2). Exposed surfaces were periodically characterized by microscopic/spectroscopic techniques and the leaching rain was monthly collected, in order to evaluate the release of the alloying metals. At the same time, a similar set of samples was exposed in a climatic chamber fitted by a UV light source to clearly discriminate the effects of thermal and UV cycling.

2. Materials and methods

2.1 Materials

Quaternary bronze coupons of the EN 1982-G85, UNS-C83600 alloy (Cu: 88.8 / Zn: 2.4 / Sn: 4.4 / Pb: 3.9 wt%) with a cored dendritic microstructure (Sn microsegregation, Sn-rich eutectoid at the periphery of dendrites, scattered Pb globules and some porosity, as described with more details in [1,2]) were used as substrates.

The precursor used to produce the protective coating on bare bronze coupons was 3-mercapto-propyl-trimethoxy-silane (PropS-SH, purity 95%, Aldrich cod. 175617), selected on the basis of a previous work [13]. The PropS-SH prefilming solutions containing or not containing 250 ppm of CeO_2 (nano-sized, Aldrich cod. 544841), TiO_2 (nano-sized, Aldrich cod. 718467), and La_2O_3 (micro-sized, Aldrich cod. 199923) oxide particles were prepared under controlled conditions. In particular, an acidic (pH~4, by addition of some drops of a diluted sulfuric acid solution) hydro-alcoholic solution of PropS-SH was prepared (90vol%/5vol%/5vol%-ethanol/water/silane; absolute ethanol, Fluka Cod. 02860). The solution was stored at 5 °C in

order to increase its shelf life. The solution was used at room temperature (RT) after at least 20 days of storage to reach a proper silane hydrolysis, but storage was never extended over 3 months to avoid undesirable condensation phenomena [42]. In fact, no variation of the coating performances was detected within a storage time interval of 20-90 days. Finally, for oxide particle-containing coatings, these particles were admixed and the suspensions were ultrasonicated for 10 min before use.

The silane coatings, with or without the oxide particles, were obtained by 1h immersion of bronze specimens in the prefilming solutions followed by fast withdrawal. A RT curing period of 10 days was always ensured, before coating exposure and analysis.

2.2 Tests

2.2.1 Weathering method: natural exposure

Natural exposure was performed on uncoated and silane-coated samples of quaternary bronze. The site chosen for the exposure was in the coastal town of Rimini, close to an environmental monitoring station. In this site, the recorded annual rainfall is, on average, about 600 mm/yr and the total annual solar radiation is about 1430 KWh/m^2. According to the international standard ISO 9223:2012 [43], the environment of exposure can be classified in the classes: $t_{3/4}$ (time of wetness about 2500 h/yr), P_0 (SO_2 concentration< 5 μg/m^3), S_1 (Cl^- dry deposition 3-60 mg/(m^2d)), urban (on the basis of NO_2 concentration, in the range 20-150 μg/m^3) and urban/industrial (on the basis of PM_{10} concentration, 30-70 μg/m^3). According to the previous version of the international standard ISO 9223, this atmosphere is considered to have a medium corrosivity towards copper and zinc.

The specimens, sized 2.5 x 5 x 0.5 cm^3, were protected on the rear by an insulating acrylic lacquer and exposed, inclined at 45° and facing South, in suitably designed racks made of PTFE on a wooden stand. Samples were exposed both in sheltered and unsheltered conditions for 13 months. As regards the unsheltered specimens only, the racks were designed in order to allow

the monthly collection of the leaching rain, in order to evaluate the release of the alloying metals.

SEM/EDS observations were carried out on all the exposed surfaces at the end of the tests.

2.2.2 Weathering method: climatic chamber

The protection efficiency against UV radiation was examined using a climatic chamber fitted with a UV light source. The lamps emit predominantly UV radiation at a wavelength of 360 nm. The irradiation is performed using 125W lamp placed inside the climatic chamber, 20 cm away from specimens. Silane-coated samples underwent 10 cycles in climatic chamber (Angelantoni, DY340) at a constant relative humidity of 70%. Each cycle consisted of 12 hrs: 4 hrs at 35 °C and 4 hrs at 0°C, with 2 hrs for each temperature ramp. The UV lamp was switched on for 2 hrs, during the section of the cycle at 35°C. During the tests, half of each sample was screened from UV exposure, in order to discriminate the contribution of UV radiation from that of thermal cycling.

2.3 Characterization

During both natural and artificial exposure tests, the bronze surfaces were characterized as a function of exposure time. The composition of the patina was identified by a hyphenated system SEM-EDS-Raman (Zeiss EVO 50 EP (extended pressure) apparatus coupled both with an EDS microprobe (software INCA 350, Oxford Energy) and a Raman spectroscope (Renishaw InVia connected by Renishaw SCA, Structural and Chemical Analyser, λ = 514.5 nm, 50 mW) as well as by X-Ray Diffraction (Philips Diffractometer PW 1729, 40 kV/30 mA, Cu Kα radiation).

In unsheltered natural exposure, the collected rain was periodically analysed by Graphite Furnace Atomic Absorption Spectrometry (GF-AAS, Perkin-Elmer AAnalyst 400) as described in [2]. The efficiency of PropS-SH in terms of inhibition of metal release in the rain was quantified through the analyses of the metals dissolved in the ageing solution. Specifically, the

Inhibiting Efficiency in terms of Metal Release (IEMR, %) for each alloying element and for the whole alloy was calculated using eqn. (1):

$$IEMR = \frac{M_{sol,NC} - M_{sol,C}}{M_{sol,NC}} x\ 100 \quad (1)$$

Where: M is the considered metal, M_{sol} is the amount of metal leached in the rain solution (i.e. Cu, in μg cm^{-2}); NC is the non-coated and C is the coated coupon. Therefore, IEMR is 100% if no metal is released from the coated coupon, and 0% if the coated coupon releases as much metal as the uncoated one.

The coated samples exposed to climatic chamber were also analyzed by specular reflectance FT-IR spectroscopy (Nicolet 550 Magna II), with a fixed 80° grazing angle accessory and a mercury cadmium telluride (MCT) detector, before and after the exposure to UV/thermal cycles in climatic chamber, in order to detect structural modification of the silane coatings.

Differential scanning calorimetry (Perkin Elmer, DSC6) analysis was carried out in order to register silanes thermal transitions. Scanning rate of 20 °C/min, nitrogen flow of 20 ml/minand temperature range of -70÷150 °C were used as operative conditions. Aluminium pans were filled with ≈ 4-5 mg of silanes, with or without the oxide particles, and tested before and after the exposure to UV/thermal cycles in climatic chamber.

Finally, colorimetric measurements were performed in the CIELAB Space through Datacolor Check II (illuminant D65, 10°observer, beam of diffuse light of 6 mm). In this system, the difference between two colours is expressed by the ΔE parameter: $\Delta E = \sqrt{(\Delta L^{*2} + \Delta a^{*2} + \Delta b^{*2})}$, where L^*, a^* and b^* represent the lightness, the red/green and the yellow/blue axis, respectively.

3. Results and discussion

3.1 Natural Ageing

Fig. 1 shows a comparison of macroscopic images of the samples after natural exposure (13 months, sheltered/unsheltered samples). Qualitative differences between the uncoated and

coated bronze specimens are clearly visible in Fig. 1, which also highlights the beneficial influence of the oxide particles added to PropS-SH, mostly in the case of TiO_2.

Fig. 2 shows the high-magnification SEM images of aged bronze surfaces as a function of exposure geometry (sheltered vs. unsheltered), after 13 months of natural exposure in the coastal site of Rimini. Higher magnification details with X-ray EDS maps are shown in Fig. 3 for PropS-SH in sheltered conditions.

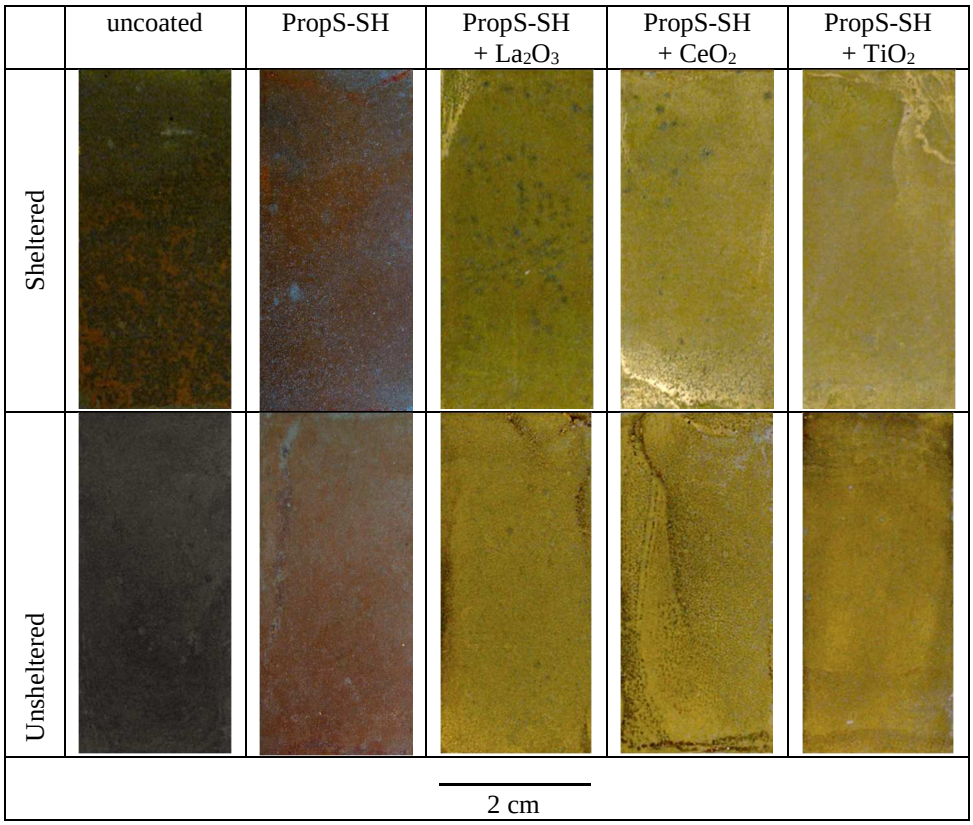

Fig. 1: Macroscopic images of samples after natural exposure (13 months).

	Sheltered	Unsheltered

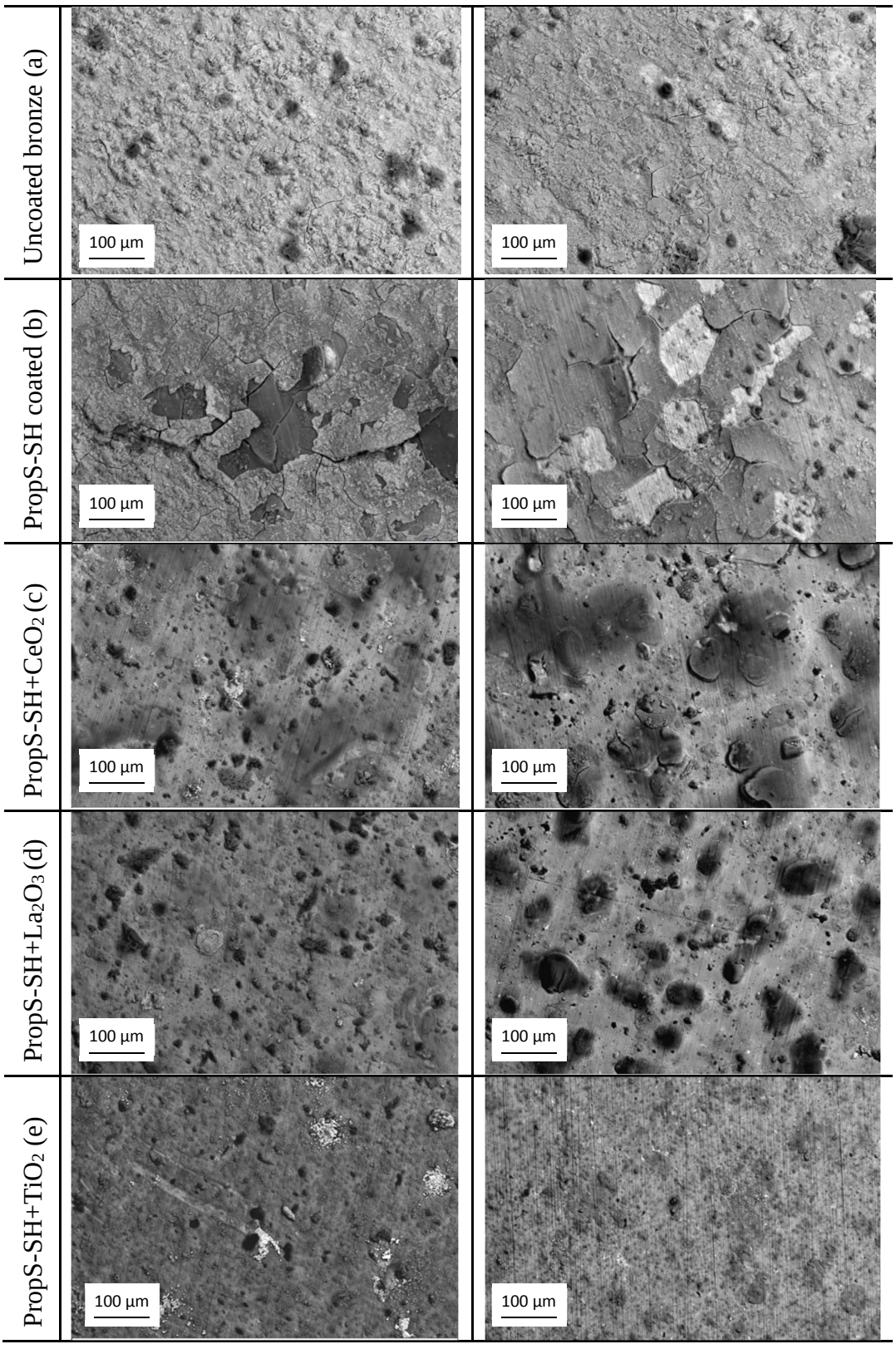

Fig. 2: SEM-BSE images of corroded bronze surfaces after 13 months of natural exposure under sheltered (left images) and unsheltered (right images) conditions (500X): uncoated (a) and PropS-SH coated (b-e) specimens (plain PropS-SH (b); PropS-SH+CeO_2(c); PropS-SH+La_2O_3 (d); PropS-SH+TiO_2 (e)).

On PropS-SH-coated bronze (Fig. 2b), cracking and spalling of the silane coating were observed. In particular, in the detachment area of sheltered samples (Fig. 3), corrosion products started to grow on the metal substrate. In these samples, the surface coating has a double-layer structure, consisting of an internal layer of PropS-SH (indicated by an arrow) and an external layer of PropS-SH mixed with corrosion products and deposits, as shown by the X-Ray maps in Fig. 3.

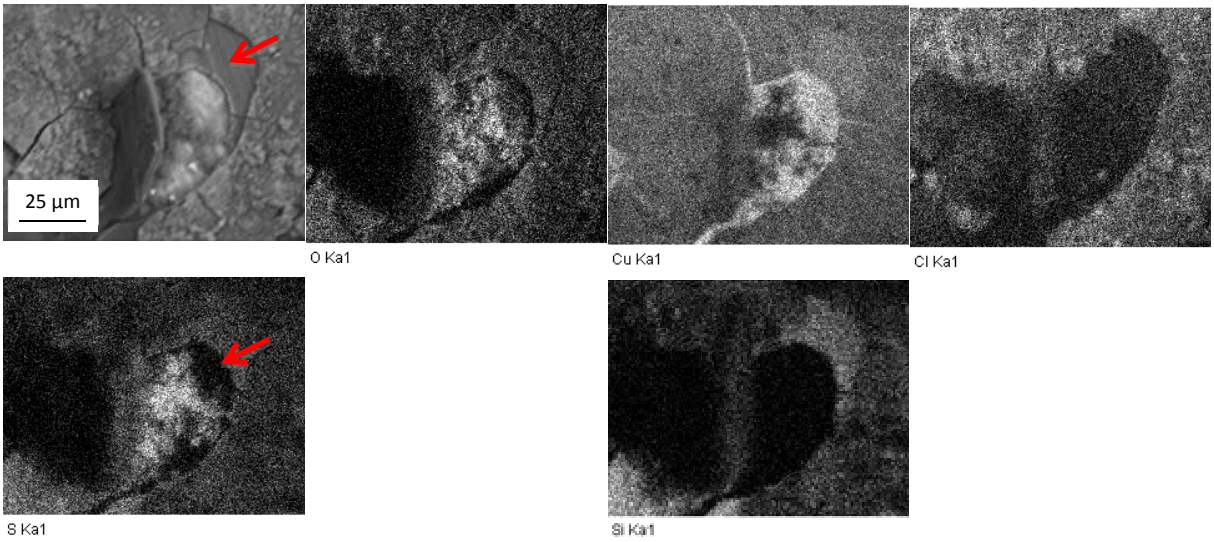

Fig. 3: EDSX-Ray maps of the surface of PropS-SH coated bronze after 13 months of natural exposure, under sheltered exposure conditions. The arrow in the SE image indicates the internal layer of PropS-SH.

Unsheltered exposure conditions generally lead to a higher incidence of spalling by comparison to sheltered conditions (Fig. 2), due to the chemical-mechanical action of the rainwater and to the higher irradiation energy. By comparison to the sheltered ones, in the unsheltered samples only a single layer of PropS-SH is visible (Fig. 4), probably due to the leaching action of rainwater, which did not allow the persistence of the outer cracked deposition layer. From these SEM observations the thickness of PropS-SH could be also estimated and corresponded to about 3-4 µm.

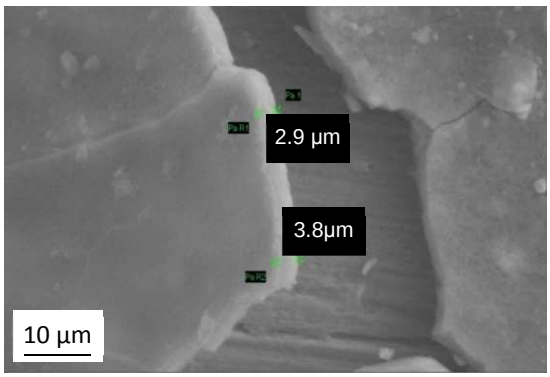

Fig. 4: BSE image (4000X) of PropS-SH coated bronze surfaces after 13 months of natural exposure, under unsheltered conditions.

After 13 months of exposure, the specimens protected by oxide particle-charged coatings showed a reduced spalling phenomenon on both sheltered and unsheltered exposure conditions, especially in the case of TiO_2 (Fig. 2e).

On coupons with ceria- and lanthania-charged coatings (Fig. 5a,b), small exfoliation sites were visible at higher magnification, where EDS demonstrated the local coating removal. On the contrary, in the case of titania-charged coatings (Fig. 5c), localised SEM-EDS analyses highlighted much smaller defects where the protective coating was still present.

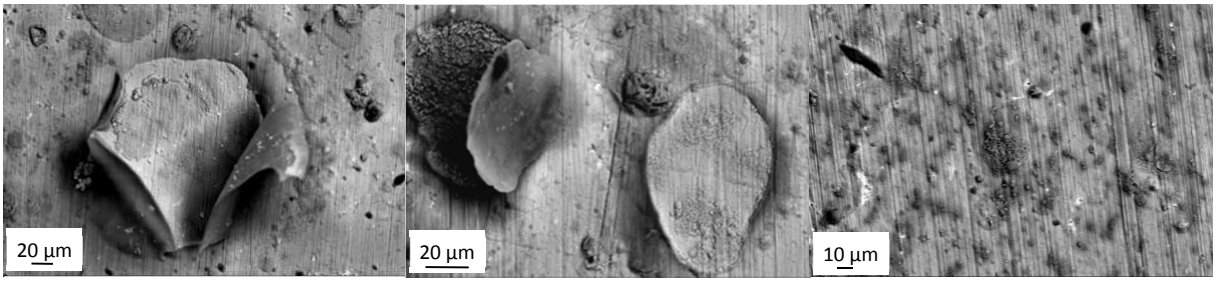

Fig. 5: SEM-BSE images of defects on (a) PropS-SH+CeO_2, (b) PropS-SH+La_2O_3, (c) PropS-SH+TiO_2 coatings after 13 months of natural exposure, under unsheltered conditions.

At the end of the exposure period, while on uncoated bronze cuprite, nantokite and posnjakite were detected by XRD and Raman micro-spectroscopy in the corrosion products, all the coated samples only showed the presence of cuprite. This suggests that, in spite of the above described local micro-damages, all PropS-SH-based coatings partially restricted the formation and evolution of corrosion products.

As regards metal release from PropS-SH-coated surfaces in unsheltered conditions, the leaching rain analysis showed that during the13 months of exposure the application of the silane coating induced a decrease of copper dissolution. Specifically, the average monthly Inhibition Efficiency in terms of Cu Release ($IEMR_{Cu}$, eqn. (1)) for plain PropS-SH was around 30%, while the addition of nano-sized particles to the silane coating lead to an increase of the average monthly $IEMR_{Cu}$ up to 45%.

Considering that the IEs derived from both electrochemical tests and accelerated ageing tests reported in [12,14,15] and related to 10 day-cured coatings ranged from 70 to 98%, this efficiency decrease is probably due to the synergistic effect of the environmental conditions and in particular to the influence of the UV component of solar radiation and thermal cycles, not taken into account in previous tests. Therefore, in the next section, the results of accelerated ageing tests by climatic chamber with UV radiation and thermal cycles are presented and discussed.

3.2 Climatic chamber (UV + Thermal cycles)

So as to separately evaluate the influence of temperature and UV radiation on the corrosion behavior of PropS-SH-coated surfaces, during thermal/UV cycles in climatic chamber half of each sample was UV-screened. At the end of the test, macroscopic observations showed a visible yellowing on all areas exposed to UV radiation (Fig. 6). The TiO_2-charged coating was the least affected by this phenomenon. Colorimetric measurements confirmed the visual observation. In fact, colour variations for samples exposed only to thermal cycles were always lower than 2, so not significant considering that a $\Delta E=3$ is assumed as the perceptibility threshold in the field of cultural heritage [15]. On the contrary, among samples exposed to thermal/UV cycles only TiO_2-charged coating revealed a ΔE equal to 3 ± 2, while the other

coatings presented higher values (up to 10, in the case of plain PropS-SH and PropS-SH+La_2O_3).

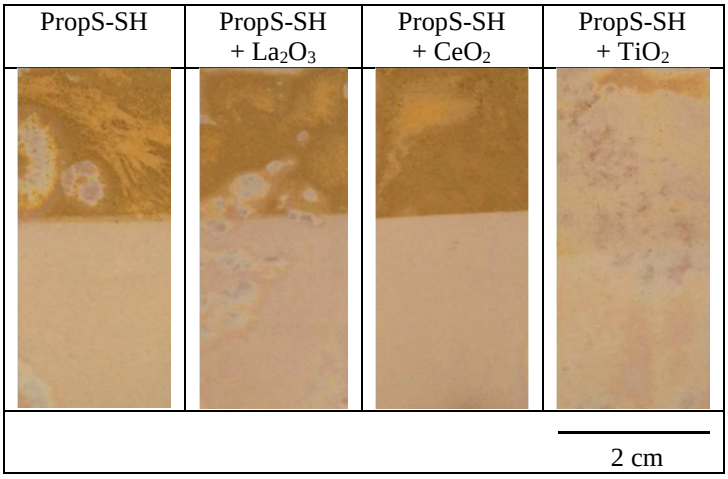

Fig. 6: Macroscopic images of samples after UV/T cycles in climatic chamber. The lower half of each sample (lighter area) was screened from UV radiation, whilst the upper half was exposed to both UV radiation and thermal cycles.

SEM observations showed that on silane-coated specimens many white globules are always visible which correspond to the Pb globules of the quaternary alloy. Uncharged PropS-SH coatings underwent localized exfoliation in areas exposed to UV (Fig. 7a), particularly where the coating was thicker. In the presence of oxide particles these exfoliations are rare, particularly when TiO_2 particles are added to the coating (Fig. 7b), suggesting an improvement against the coating degradation. On UV–screened surfaces, this kind of alteration was never observed, indicating a negligible influence of thermal cycles on silane degradation.

The combined action of thermal and UV cycles induced a peculiar modification of the polymeric film. In fact, the formation of dark rounded spots was observed mainly on PropS-SH (indicated by arrows in Fig. 7a) and PropS-SH+ La_2O_3, while they were much less pronounced in the presence of CeO_2 and TiO_2 (Fig. 7b). These spots are clearly connected to the photo-induced degradation of the coatings.

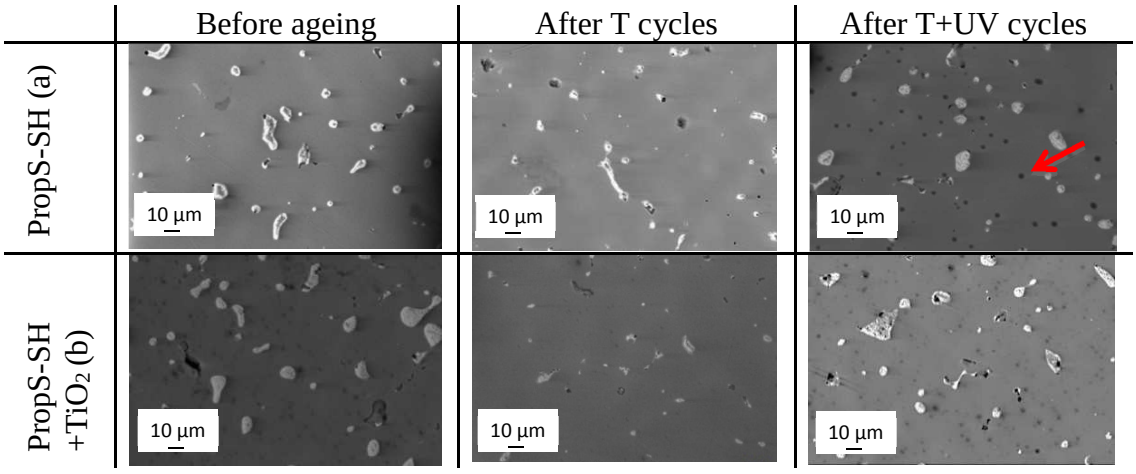

Fig. 7: SEM-BSE images (2000X) of PropS-SH (a) and PropS-SH+TiO_2 (b) coated bronze before and after thermal and UV ageing by climatic chamber. The arrow indicate the dark rounded spots discussed in the text.

To get into this point, a characterization of the aged PropS-SH-coated surfaces and PropS-SH-based coatings was performed through FTIR spectroscopy, XRD, as well as Differential Scanning Calorimetry (DSC).

3.3 FTIR Spectroscopy

Fig.8 shows a comparison among the FTIR spectra collected on 10 day-cured coatings, before (spectrum 1, green) and after ageing, that is after thermal cycles (spectrum 2, blue) or UV-thermal cycles (spectrum 3, red).

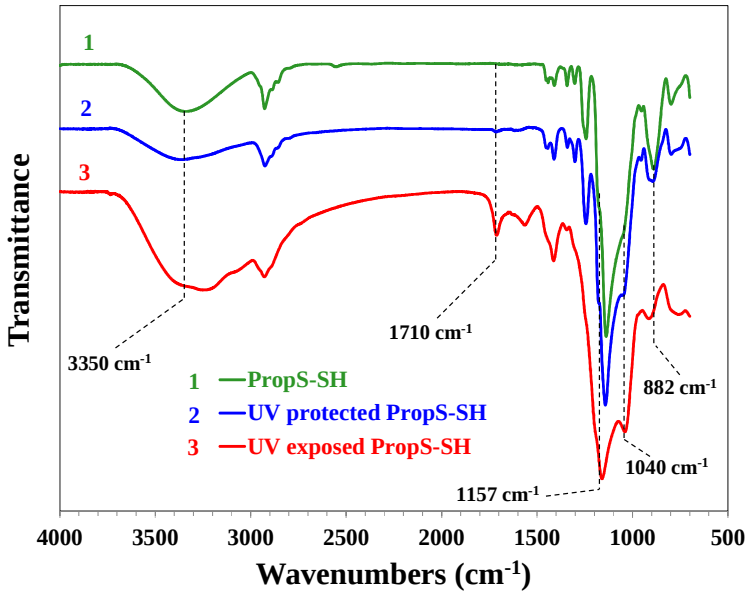

Fig. 8: FTIR spectra of PropS-SH coatings before ageing (spectrum 1), after thermal ageing in UV-protected areas (spectrum 2) and after thermal ageing in UV-exposed regions (spectrum 3).

Considering as a reference the spectrum of the 10 day-cured silane coating, it can be noticed that thermal ageing produces a decrease in the intensity of the peaks at 3350 and 882 cm^{-1} (corresponding to the symmetric stretching of O-H and Si-OH bonds, respectively), if compared to the band between 1200 and 1000 cm^{-1}corresponding to the Si-O-Si polysiloxane asymmetric stretching [18,44,45].

These variations could be explained as the evolution of the system from hydrolysed silane into a reticulated configuration, characterized by cage-like (peak at 1157cm^{-1}), cyclic (peak at 1040cm^{-1}) and long open chain (broad bands between 1090 and 1020 cm^{-1}) polysiloxane structures [44-46].

While the thermal cycles accelerate the 3-D reticulation, the UV radiation seems to cause damages in the siloxane structure. In particular, as also suggested by Bao et al. [26], breakages of the Si-C bonds and conversion into silanol groups are suggested by the more intense band observed in spectrum 3 between 3700 and 3200 cm^{-1}, connected to O-H stretching, and the increased peak at 1411cm^{-1}, attributed to OH bending [47]. Fig. 8 also highlights that this is accompanied by photo-oxidation of the hydrocarbon chains of PropS-SH, as revealed by the

onset of a peak at 1710 cm^{-1}, connected to the formation of carbonyl groups [26,27,48,49]. The partial decomposition of the polysiloxane net is expected to produce degradations products with shorter chain length, which could be responsible of the appearance of the small round dark spots observed after thermal/UV cycles and shown in Fig. 7.

Concerning the influence of oxide particles on the performance of PropS-SH under UV/thermal cycling, in Fig.9 FTIR spectra obtained after thermal cycling on UV-protected (a) or UV-exposed (b) areas are compared. The spectra obtained after only thermal cycling (Fig.9a) are very close to each other, while differences are detected after UV irradiation (Fig. 9b). In particular, oxide particles appear to afford a beneficial influence against degradation, because IR spectra show: (i) a decreasing band intensity for OH stretching according to the following order: PropS-SH > PropS-SH+CeO_2 > PropS-SH+La_2O_3 > PropS-SH+TiO_2 (indicating a decreasing tendency to Si-C bond breakage and silanol group formation in the presence of the different particles, particularly TiO_2); (ii) a lower relative intensity of the band at 1040 cm^{-1} (cyclic polysiloxane or long open-chain groups), with respect to that at 1157 cm^{-1} (cage-like polysiloxanes) [44] in the presence of particle-charged silane (suggesting a higher reticulation degree when particles are added); (iii) a smaller intensity of the peak at 1710 cm^{-1}, connected to the hydrocarbon chain photo-oxidation, in particle-charged silane coatings and particularly in the case of TiO_2.

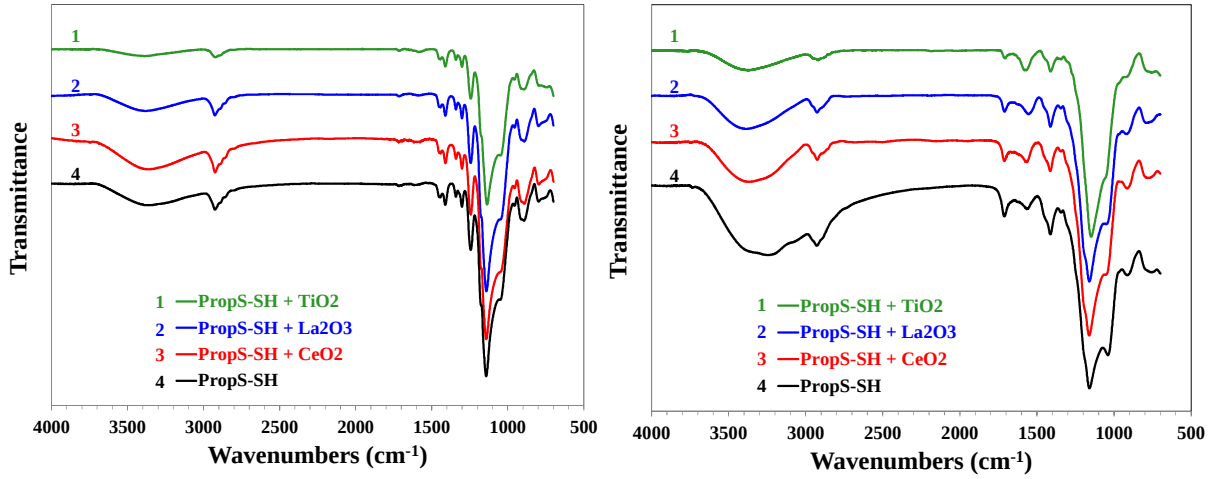

Fig. 9: FTIR spectra measured on PropS-SH coatings with or without metal oxide particles: (a) after thermal cycles; (b) after thermal/UV cycles.

XRD patterns for plain PropS-SH-coated bronze are compared in Fig. 10, so as to highlight the influence of exposure to thermal cycles and UV radiation on the structure of the organo-silane layer. The main contributions to these XRD patterns are due to the substrate (the most intense peaks being attributed to the Cu-rich matrix, with less intense peaks due to Pb globules). However, the sample exposed to accelerated ageing with thermal cycles (no UV) shows the presence of broad diffraction bands at low 2θ angles (boxed area in Fig. 10), due to basal spacing corresponding to d=0.58 nm and d=0.39 nm, respectively. These bands, likely related to partially crystalline phases, are compatible with the mercaptopropyl-siloxane chain length (~ 0.6 nm) and (200)/($\bar{1}$11) plane spacings of cristobalite (82-1560 ICDD-PDF), respectively. Therefore, these patterns may be related to thermal induced structural modifications of the silane network conformation, due to the organization in layered structures, where the basal spacings correspond to the distances of these layers.

The peaks and bands related with silane structure modifications are not detectable after addition of UV radiation, suggesting that the high severity of such exposure conditions leads to a more disordered silane structure.

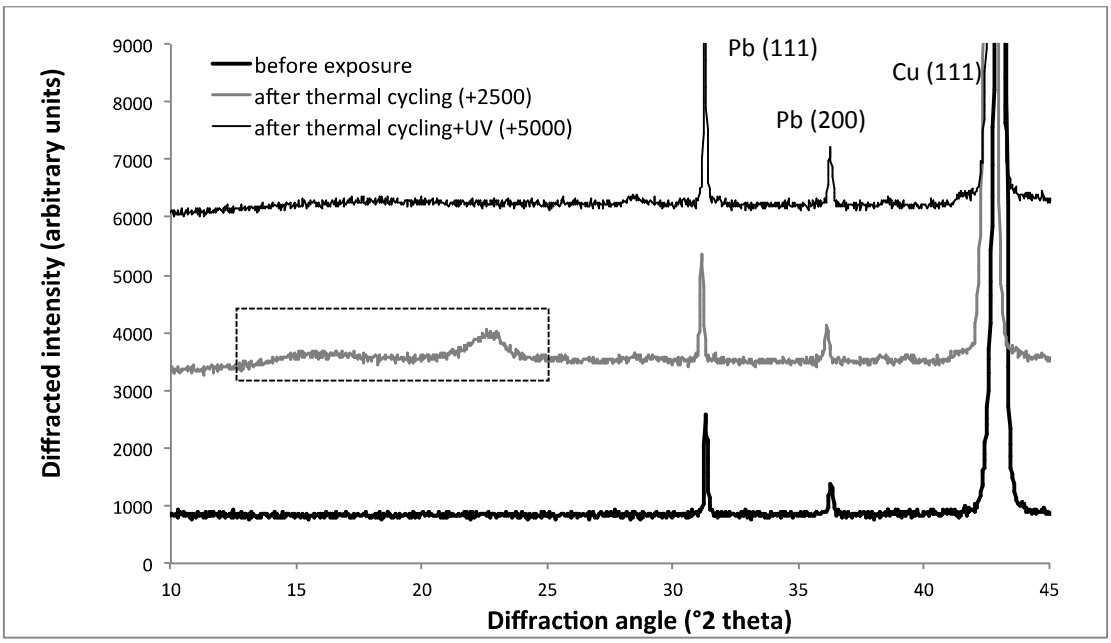

Fig. 10: XRD spectra (Cu Kα) measured on the PropS-SH coated bronze before climatic chamber exposure, after thermal cycling and after thermal cycling +UV. The boxed area in the XRD pattern of the thermally cycled sample (pattern 2) is discussed in the text.

Thermal analysis of PropS-SH before and after the exposure to UV/thermal cycles in climatic chamber is reported in Fig. 11 together with the DSC curves relevant to the oxide-based silanes after UV/thermal cycles. PropS-SH (1) exhibits a glass transition temperature, T_g, at -50 °C and, except a very slight inflection at ≈ 33 °C, no other thermal transitions are evident. A similar behaviour was detected for the oxide-based silanes before the UV/thermal treatment (not showed): all the samples exhibit the same transitions in the range of -50 ÷ -45 °C and 33-35 °C, respectively.

After the UV/thermal cycles, some changes occur in the recorded DSC thermograms. In PropS-SH (2) the glass transition temperature is shifted towards higher values and a broad peak associated to an endothermic transition is clearly visible. The same trend is shown by the oxide-charged PropS-SH (3,4,5), however the peak as well as the increase of T_g become less evident, according to the following order: PropS-SH+CeO_2 > PropS-SH+La_2O_3 > PropS-SH+TiO_2.

The broad peak detected in PropS-SH after UV/thermal cycles can be ascribed to low melting oligomers formed during the degradation process induced by UV, in agreement with the

suggestions of FTIR analysis (breakage of polysiloxane bonds, indicated by the relative increase of peaks connected to silanol groups with respect to those connected to polysiloxane bonds). These degradation products could be responsible of the more disordered structure detected by XRD analysis on UV-irradiated silane samples.

In the presence of particle-charged silane, both the decrease of the endothermic peak intensity and the shift towards more negative values of the T_g (if compared to that measured on plain PropS-SH) point to a higher resistance to degradation. In particular, the latter finding indicates that the reticulated silane remains flexible in a wider temperature range, due to the persistence of a more continuous net of polysiloxane bonds.

FTIR and DSC tests results suggest that the studied oxide particles improve the PropS-SH coating performances against UV/thermal degradation mainly by assisting silane reticulation. More specifically, a more densely polymerized silane structure appears less prone to photodegradation. Titania was the most effective oxide particle type, likely because beside a net forming capability it also afforded a specific activity as a UV light absorber.

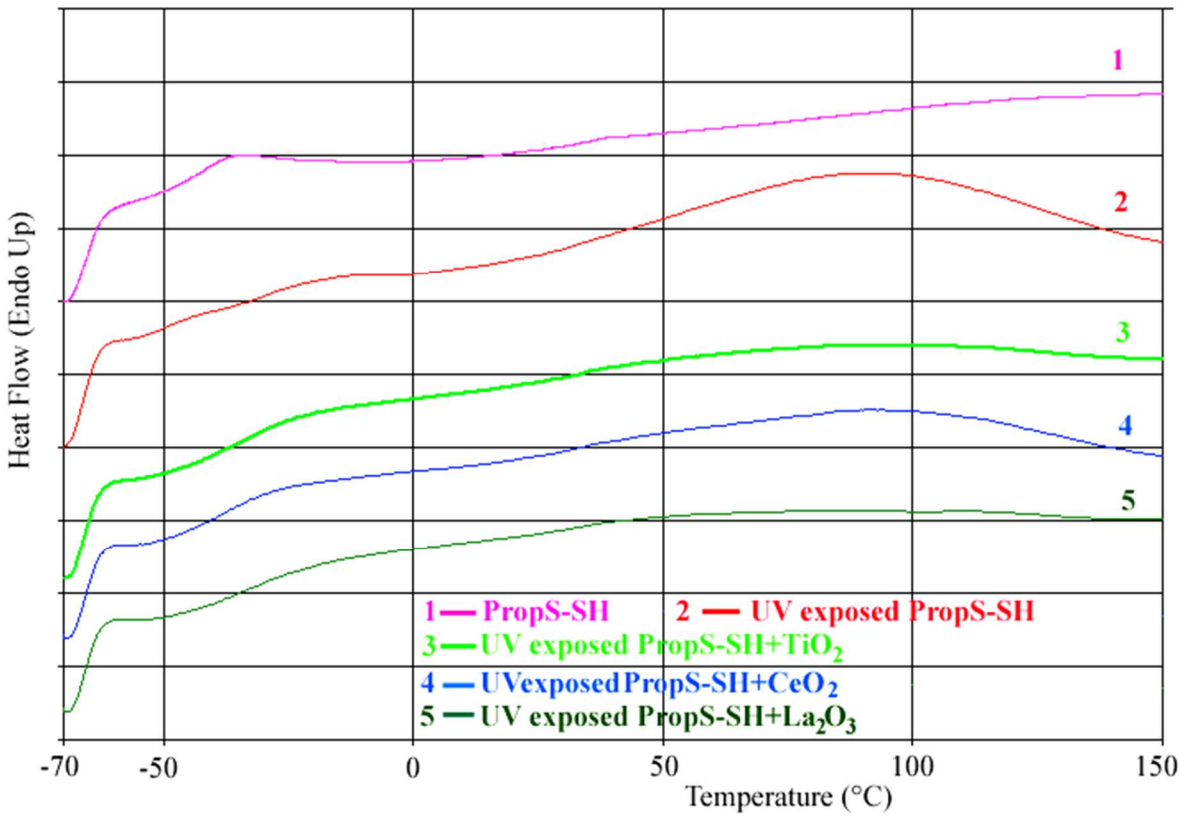

Fig. 11: DSC analysis of PropS-SH silanes. Before ageing: PropS-SH (curve 1); after UV/thermal ageing in climatic chamber: PropS-SH (curve 2), PropS-SH+TiO_2 (curve 3), PropS-SH+CeO_2 (curve 4), and PropS-SH+La_2O_3 (curve 5).

4. Conclusions

The results showed that on silane based coatings micro-scale cracking and spalling phenomena take place during natural exposure, partly limiting their protective efficiency. The addition of oxide particles slightly reduced the tendency towards spalling, especially in the case of TiO_2, which also ensured negligible color changes. Exposure to temperature/UV cycles showed that while thermal cycles in humid atmosphere stimulate silane reticulation, UV radiation is responsible of the degradation process of the silane net and the impairment of the coating performances. Degradation is connected to breakage of polysiloxane bonds and photo-oxidation which induced formation of silanol and carbonyl groups.

These tests indicate that the improvement of the PropS-SH coating stability under UV exposure afforded by dispersed oxide particles is mainly connected to their capability to act as network formers. Photostability is highest in the presence of TiO_2 nanoparticles, likely because, beside their contribution to silane polymerization, they can absorb UV radiation so reducing more significantly the coating damage.

These findings suggest testing more extensively anti-UV additives, such as TiO_2 and others, in order to improve the UV resistance of silane and guarantee the protected surfaces a natural aspect. Also addition of lanthania nanoparticles (instead of microparticles) could give improved coating performances. In fact, nanoparticles can be more finely distributed in the coatings and can introduce a higher density of bridges in the silane network.

Acknowledgements

The financial support of Emilia-Romagna Region (POR-FESR funds) and MIUR (PRIN 2009) is gratefully acknowledged. The authors are also grateful to Dr. M. Abbottoni for the preparation of the silane coatings.

Reference list

[1] E. Bernardi, C. Chiavari, B. Lenza, C. Martini, L. Morselli, F. Ospitali, L. Robbiola, The atmospheric corrosion of quaternary bronzes: The leaching action of acid rain, Corros Sci. 51 (2009) 159-170.

[2] C. Chiavari, E. Bernardi, C. Martini, F.Passarini, F. Ospitali, L. Robbiola, The atmospheric corrosion of quaternary bronzes: the action of stagnant rain water, Corros Sci. 52 (2010) 3002-3010.

[3] E. Joseph, P. Letardi, R. Mazzeo, S. Prati, M. Vandini, Innovative Treatments for the Protection of Outdoor Bronze Monuments, in: C. Degrigny, R. van Langh, I. Joosten, B.Ankersmit (Eds.) Metal 2007, Rijksmuseum, Amsterdam, 2007, pp. 71-77.

[4] V. Balek, Z. Malek, B. Casensky, D. Niznansky, J. Subrt, E. Vecernikova, H. Romich, M. Pilz, A New Approach to Characterization of Barrier Properties of ORMOCER Protective Coatings, Journal of Sol-Gel Science and Technology 8 (1997) 591-594.

[5] P. Letardi, Laboratory and field tests on patinas and protective coating systems for outdoor bronze monuments, Proc. of Metal 2004, Canberra, Australia, 04-08/10/2004, p. 379-387.

[6] G. Bierwagen, T.J. Shedlosky, K. Stanek, Developing and testing a new generation of protective coatings for outdoor bronze sculpture, Progr. Org Coat. 48 (2003) 289–296.

[7] E. Bescher, J.D. Mackenzie, Sol-Gel Coatings for the Protection of Brass and Bronze, J Sol-gel Sci Tech. 26, 2003, 1223–1226.

[8] A. Frignani, F. Zucchi, G. Trabanelli, V. Grassi, Protective action towards aluminium corrosion by silanes with a long aliphatic chain, Corros Sci. 48 (2006) 2258–2273.

[9] F. Deflorian, S. Rossi, L. Fedrizzi, Silane pre-treatments on copper and aluminum, Electrochim Acta 51 (2006) 6097 – 6103.

[10] F. Zanotto, V. Grassi, A. Frignani, F. Zucchi, Protection of the AZ31 Magnesium alloy with cerium modifiedsilane coatings, Mat Chem Phys. 129 (2011) 1–8.

[11] S.H. Zaferani, M. Peikari, D. Zaarei, I. Danaee, J.M. Fakhraei, M. Mohammadi, Using Silane Films to Produce an Alternative for Chromate Conversion Coatings, Corrosion, 69, 4 (2013) 372-387.

[12] A. Balbo, A. Frignani, C. Monticelli (2012), “Influence of nanoparticles on the inhibiting efficiency of organosilane coatings on bronze. Part 1: Electrochemical characterization”, Proc. Eurocorr 2012 (EFC Event n.330), 09-13/09/2012, Istanbul, Turkey (2012) EFC, London, UK (CD-ROM) Paper 1524, p.1-8.

[13] A. Balbo, C. Chiavari, C. Martini, C. Monticelli, Effectiveness of corrosion inhibitor films for the conservation of bronzes and gilded bronzes, Corros Sci. 59 (2012) 204–212.

[14] C. Chiavari, E. Bernardi, A. Balbo, C. Monticelli, F. Passarini, M.C. Bignozzi, C. Martini, Influence of nanoparticles on the inhibiting efficiency of organosilane coatings on bronze. Part 2: metal release in accelerated ageing tests, Proc. Eurocorr 2012, 09-13/09/2012, Istanbul, Turkey, Paper n.1498, p.1-11.

[15] C. Chiavari, A. Balbo, E. Bernardi, C. Martini, M.C. Bignozzi, M. Abbottoni, C. Monticelli, Protective silane treatment for patinated bronze exposed to simulated natural environments, Mat Chem Phys. 141, 1 (2013) 502-511.

[16] F. Zucchi, A. Frignani, V. Grassi, G. Trabanelli, M. Dal Colle, The formation of a protective layer of 3-mercapto-propyl-trimethoxy-silane on copper, Corros Sci 49 (2007) 1570–1583.

[17] Y.-S. Li, W. Lu, Y. Wang, T. Tran, Studies of (3-mercaptopropyl)trimethoxylsilane and bis(trimethoxysilyl)ethane sol–gel coating on copper and aluminum, Spectrochim Acta Part A 73 (2009) 922–928.

[18] M.-A. Chen, X.-B.Lu, Z.-H.Guo, R. Huang, Influence of hydrolysis time on the structure and corrosion protective performance of (3-mercaptopropyl)triethoxysilane film on copper, Corros Sci. 53 (2011) 2793–2802.

[19] F. Zucchi, V. Grassi, A. Frignani, G. Trabanelli, C. Monticelli, Octadecyl-trimethoxy-silane film formed on copper in different conditions, Mat Chem Phys.103 (2007) 340–344.

[20] F. Deflorian, S. Rossi, L. Fedrizzi, M. Fedel, Integrated electrochemical approach for the investigation of silane pre-treatments for painting copper, Progr Org Coat. 63 (2008) 338–344.

[21] C. Rahal, M. Masmoudi, M. Abdelmouleh, R. Abdelhedi, An environmentally friendly film formed on copper: Characterization and corrosion protection, Progress in Organic Coatings 78 (2015) 90–95.

[22] H. Zhu, S. Chen, Y. Chen, Z. Zhu, Y. Yin, Investigation of the corrosion resistance of n-tetradecanoic acid and its hybrid film with bis-silane on copper surface in seawater, J. Mol. Struct. 928 (2009) 40–45.

[23] M. Pilz, H. Römich, Sol-Gel Derived Coatings for Outdoor Bronze Conservation, J Sol-gel Sci Tech. 8, 1071–1075 (1997).

[24] W.J. van Ooij, D. Zhu, M. Stacy, A. Seth, T. Mugada, J. Gandhi, P. Puomi, Corrosion protection properties of organofunctional silanes–an overview, Tsinghua Sci. Tehnol. 10 (2005) 639–666.

[25] G. Gupta, S.S. Pathak, A.S. Khanna, Anticorrosion performance of eco-friendly silane primer for coil coating applications, Progr Org Coat. 74 (2012) 106–114.

[26] J.-Q. Bao, Q. Wang, X. Liu, L. Ding, Site-selective deposition of copper by controlling surface reactivity of SAMs with UV-irradiation, Surf Sci. 602 (2008) 2250–2255.

[27] A.P. Kumar, D. Depan, N.S. Tomer, R.P. Singh, Nanoscale particles for polymer degradation and stabilization—Trends and future perspectives, Prog Polym Sci. 34 (2009) 479–515.

[28] R. Yang, P.A. Christensen, T.A. Egerton, J.R. White, Degradation products formed during UV exposure of polyethylene-ZnOnano-composites, Polym Degrad Stab. 95 (2010) 1533-1541.

[29] H. Zhao, R.K.Y. Li, A study on the photo-degradation of zinc oxide (ZnO) filled polypropylene nanocomposites, Polymer 47 (2006) 3207–3217.

[30] S.S. Pathak, A.S. Khanna, T.J.M. Sinha, HMMM cured corrosion resistance waterborne ormosil coating for aluminum alloy, Progr Org Coat. 60 (2007) 211–218.

[31] D.K. Hwang, J.H. Moon, Y.G. Shul, K.T. Jung, D.H. Kim, D.W. Lee, Scratch resistant and transparent UV-protective coating on polycarbonate, J Sol-Gel Sci Tech. 26, (2003) 783–787.

[32] X.D. Chen, Z. Wang, Z.F. Liao, Y.L. Mai, M.Q. Zhang, Roles of anatase and rutile TiO_2 nanoparticles in photooxidation of polyurethane, Polymer Testing 26 (2007) 202–208.

[33] M.F. Montemor, W. Trabelsi, S.V. Lamaka, K.A. Yasakau, M.L. Zheludkevich, A.C. Bastos, M.G.S. Ferreira, The synergistic combination of bis-silane and $CeO_2 \cdot ZrO_2$ nanoparticles on the electrochemical behaviour of galvanised steel in NaCl solutions, Electrochim Acta 53 (2008) 5913–5922.

[34] H. Fan, S. Li, Z. Zhao, H. Wang, Z. Shi, Improving the formation and protective properties of La-conversion coatings on brass by use of La_2O_3 nanoparticle incorporation with electrodeposition, Corros Sci. 53 (2011) 3821–3831.

[35] Q. Chen, N.L. Yakovlev, Adsorption and interaction of organosilanes on TiO_2 nanoparticles, Appl Surf Sci. 257 (2010) 1395–1400.

[36] M.F. Montemor, R. Pinto, M.G.S. Ferreira, Chemical composition and corrosion protection of silane films modified with CeO_2 nanoparticles, Electrochim Acta 54 (2009) 5179–5189.

[37] A. Phanasgaonkar, V.S. Raja, Influence of curing temperature, silica nanoparticles- and cerium on surface morphology and corrosion behaviour of hybrid silane coatings on mild steel, Surf Coat Technol. 203 (2009) 2260–2271.

[38] F. Zucchi, V. Grassi, F. Zanotto, A. Frignani, Influence of $CeAlO_3$ nanopowder addition on the performances of silane coatings for AZ31 alloy corrosion protection, Proc. Eurocorr 2010, 13-17/09/2010, Moscow, Russia, p.1-8.

[39] P. Letardi, R. Spiniello, Characterization of bronze corrosion and protection by contact-probe electrochemical impedance measurements, Proc. of Metal 2001, Santiago, Chile, 02-06/04/ 2001, p. 316-319.

[40] P. Letardi, Laboratory and field tests on patinas and protective coating systems for outdoor bronze monuments, Proc. of Metal 2004, Canberra, Australia, 04-08/10/2004, p. 379-387.

[41] E. Franceschi, P. Letardi, G. Luciano, Colour measurements on patinas and coating system for outdoor bronze monuments, J Cult Herit 7 (2006) 166 – 170.

[42] K.A. Yasakau, J. Carneiro, M.L. Zheludkevich, M.G.S. Ferreira, Influence of sol-gel process parameters on the protection properties of sol–gel coatings applied on AA2024, Surf. Coat. Tech. 246 (2014) 6–16.

[43] ISO 9223 (2012) Corrosion of metals and alloys- Corrosivity of atmospheres - Classification, determination and estimation.

[44] Y. Qu, G. Huang, X. Wang, J. Li, Study on the Mechanism of the Formation of Polyhedral OligomericSilsesquioxanes by the 2D Correlation Infrared Spectral, J Appl Polym Sci. 125 (2012) 3658–3665.

[45] C.W. Young, P.C. Servais, C.C. Currie, M.J. Hunter, Organosilicon Polymers. IV. Infrared Studies on Cyclic Disubstituted Siloxane, J Am Chem Soc., 70 (1948) 3758-3764.

[46] L.J. Bellamy, “The infrared spectra of complex molecules”, vol. I, 3rd Ed., Wiley &Sons , New York, 1975, p. 374.

[47] D. Lin-Vien, N. B. Colthup, W.G. Fateley, J. G. Grasselli, The handbook of infrared and raman characteristic frequencies of organic molecules, Academic Press, San Diego, Ca, USA, 1991.

[48] R. Yang, P.A. Christensen, T.A. Egerton, J.R. White, Degradation products formed during UV exposure of polyethylene-ZnOnano-composites, Polym Degrad Stab. 95 (2010) 1533-1541.

[49] H. Zhao, R.K.Y. Li, A study on the photo-degradation of zinc oxide (ZnO) filled polypropylene nanocomposites, Polymer 47 (2006) 3207–3217.